IEEE Access
Multidisciplinary | Rapid Review | Open Access Journal

Received February 23, 2020, accepted March 11, 2020, date of publication March 24, 2020, date of current version April 8, 2020.

Digital Object Identifier 10.1109/ACCESS.2020.2982489

Toward Characterization of a Rectangular Groove on a Metallic Surface by Multi-Angle Light Scattering

ZHAOLOU CAO[1,2], FENPING CUI[1,2], FENGLIN XIAN[1,2], SHIXIN PEI[1,2], JINHUA LI[1,2], AND HUICHUN YE[3]

[1]Jiangsu Key Laboratory for Optoelectronic Detection of Atmosphere and Ocean, Nanjing University of Information Science and Technology, Nanjing 210044, China
[2]School of Physics and Optoelectronic Engineering, Nanjing University of Information Science and Technology, Nanjing 210044, China
[3]Department of Precision Machinery and Precision Instruments, University of Science and Technology of China, Hefei 230026, China

Corresponding author: Zhaolou Cao (zhaolou.cao@gmail.com)

This work was supported in part by the National Natural Science Foundation of China under Grant 61605081 and Grant 11605090, and in part by the Natural Science Foundation of Jiangsu under Grant BK20180799, Grant BK20180784, and Grant BK20150929.

ABSTRACT Fast quantitative characterization of a rectangular groove with sizes from sub-micrometers to micrometers on a surface has been demanding in quality control of optical elements. We report a numerical procedure for retrieval of the geometrical parameters of a rectangular groove, including width and depth, from the angular distribution of the scattered light generated by launching plane waves on the groove on a metallic surface from different propagation directions. The far-field intensity of scattering light is first obtained by numerically solving the electromagnetic problem with the modal theory. Then, a two-stage inverse modeling approach is developed to retrieve the groove parameters based on the lookup table and repulsive particle swarm optimization from multi-angle scattering light distribution that is highly sensitive to the groove parameters. Noise influences are considered in the simulation. Results suggest that our method can precisely obtain the groove parameters for noisy signals. As the measurement of light scattering can be conducted with high efficiency, it should be a powerful tool to characterize rectangle grooves on metallic surfaces.

INDEX TERMS Light scattering, groove parameter, inverse modeling, repulsive particle swarm optimization.

I. INTRODUCTION

Quantitative evaluation of surface quality is desirable in quality control of optical elements. In laser optics, surface defects lead to unexpected scattered light that may significantly affect the component's performance. A natural approach to evaluate the surface quality is based on the physical sizes of surface defects. Three-dimensional surface profiles of defects can be obtained utilizing state-of-the-art instruments, such as white light interferometry [1], [2] and atomic force microscopy [3], [4], with which surface quality can be evaluated reliably. However, the measurements suffer from low efficiency, which hinders their applications in high-volume quality control. To date, MIL-PRF-13830B [5] and ISO 10110-7: 2008 [6] are usually employed for surface inspection in industrial applications. The former standard was developed for manual inspection, where the scratch grade is determined by comparing the scratch intensity with that of golden samples. Although the inspection can be easily adapted to different samples, the measurements suffer from subjectivity and inconsistency. Scratches of the same grade on golden samples from different manufacturers exhibit different intensity when inspected by commercial instruments [7]. Comparatively, the latter standard measures the defect size rather than the intensity of scattering light, which is much more objective and suitable for automatic machine-vision-based systems. Several systems [8]–[10] have already been developed to achieve automatic inspection and evaluation of surface quality. However, to measure scratches with width less than 60 μm, the imaging resolution should be so high that

The associate editor coordinating the review of this manuscript and approving it for publication was Franco Fuschini.

it takes a long time to cover the sample surface. It is therefore desirable to develop a method that can quantitatively evaluate surface quality in a time-effective manner.

Multi-angle light scattering has been proven to be an effective tool to measure structures with sub-micrometer size, e.g. molecular weight of polymers [11]–[13] and flow cytometry [14]–[16]. In these works, the angular distribution of scattered light is regarded to be the fingerprints of sample properties. With intensity of scattered light at several angles, the structure parameters can be retrieved based on a dedicated numerical model. It inspires us to investigate the possibility of using multi-angle light scattering to objectively evaluate the surface scratches. Starting from the assumption of rectangular scratches, several works have been conducted to study the scattered light distribution generated by launching plane waves on a groove or random surface [17]–[23]. Results show that the scattered light distribution is significantly affected by the groove and surface parameters. In these works, the substrate is usually assumed to be metallic. Since metal mirrors are widely used in laser optics and reflecting telescopes, these works can be readily applied in the prediction of scattered light distribution of a rectangular scratch on metal mirrors.

However, rapid and accurate parameter retrieval from scattered light is still a difficult task in various scenarios. In a flow cytometry, analytical equations are suitable for classifying cell types rather than precisely determining cell parameters [24]. Evolutionary algorithms are believed to be capable of getting the structure parameters that agree best with measurements [25]–[28]. Machine learning techniques based on neural network have attracted much attention in various applications for its ability of nonlinear mapping. It has already been applied in parameter retrieval of single particle from scattered light [29], [30]. We have also developed a hybrid approach to retrieve the sphere parameters from scattering light based on machine learning and genetic algorithm [31]. In recent years, particle swarm optimization (PSO) that emulating from behavior of animals societies has attracted much attention in various applications for the advantage of high efficiency [32]–[35]. As the scattering light is highly sensitive to scratch parameters, PSO provides a potential approach to solving the inverse scattering problem.

In this paper, a numerical study is conducted to retrieve the geometrical scratch parameters from angular distribution of scattered light. As the lookup table narrows down the parameter space to be searched, repulsive PSO gives precise estimation of scratch parameters. The text is organized as follows. Section II and III respectively present the theory for forward and inverse scattering problem. Results and discussions are given in Section IV. Conclusions are drawn in Section V.

II. FORWARD MODELING

Assuming the surface scratch to be a rectangular groove, a monochromatic plane wave irradiates an infinitely long rectangular groove of width $2a$ and depth d on a metallic surface and generates scattered light, as shown in Fig. 1.

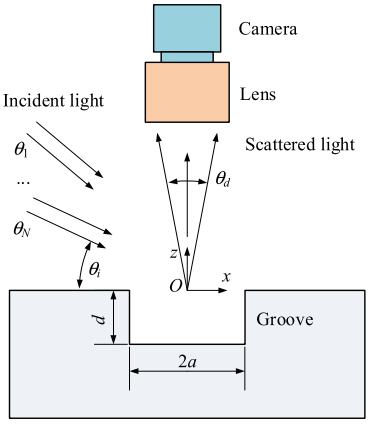

FIGURE 1. Geometry of the 2D scattering problem.

Scratches with arbitrary shapes will be studied in the future. In conventional multi-angle light scattering measurements of particles, the detector rotates around the sample to get the angular distribution of scattering light. However, it is better to fix the detector during the surface quality measurement in order to keep the detector plane and metallic surface in conjugate positions. On the other hand, although the illumination angle can be continuously adjusted by mechanically rotating a single light source by a motorized stage, we adopt the illumination provided by several plane waves that can be separately controlled for the sake of efficient measurement. Therefore, multiple plane waves with different propagation directions are employed to irradiate the groove and generate scattering light in accordance with practical measurement systems. A camera detects the scattered light inside a certain scattering angle range θ_d determined by the imaging system. Assuming N plane waves with different incident angle θ_i are used, an intensity vector $I_0 = [I_1, I_2, \ldots, I_N]$ is obtained for each groove, where I_i $(i = 1, \ldots, N)$ is the scattered light intensity for the corresponding plane wave, given by

$$I_i = \int_{-\theta_d/2}^{\theta_d/2} |E(x, z)|^2 \, d\theta, \tag{1}$$

where $E(x, z)$ is the amplitude of electric field.

Plane wave scattering by a rectangular groove has been extensively studied in the literatures, and therefore, we herein give a brief description of plane wave scattering by a rectangular groove [22].

Assuming the incident light is a *s*-polarized monochrome light and omitting the time-harmonic factor of $\exp(-i\omega t)$ associated with the field, the electric field in the upper region is given by.

$$E_y^{inc}(x, z) = \exp[j(k_x x - k_z z)], \tag{2}$$

$$E_y^{ref}(x, z) = -\exp[j(k_x x + k_z z)], \tag{3}$$

$$E_y^{sca}(x, z) = \frac{1}{2\pi} \int_{-\infty}^{\infty} \tilde{E}_y^{sca}(\xi) \exp(-j\xi x + jk_1 z) \, d\xi, \tag{4}$$

where the superscripts *inc*, *ref*, and *sca* respectively denote the incident, reflected, and scattered electric field, (k_x, k_z) are the

wave vectors in the x and z directions subject to $k_x^2+k_z^2=k_0^2$, where $k_0=2\pi/\lambda$ with λ as the wavelength, $\tilde{E}_y^{sca}(\xi)$ is the Fourier transformation of scattering field, $k_1=\left(k_0^2-\xi^2\right)^{1/2}$.

Based on modal theory, the electric field inside the groove is given by

$$E_y(x,z)=\sum_{m=1}^{\infty}c_m\sin\left[\xi_m(z+d)\right]\sin\left[a_m(x+a)\right], \quad (5)$$

where c_m is the modal amplitude, $a_m=m\pi/2a$, $\xi_n=(k_0^2-a_n^2)^{1/2}$. According to the continuity, the electric field in the upper region and inside the groove should match at $z=0$. After complicated computation, the coefficients c_n are given by

$$\mathbf{C}=(\mathbf{U}-\mathbf{P})^{-1}\mathbf{Q}, \quad (6)$$

where $\mathbf{C}$ is the column vector containing elements c_n, $\mathbf{U}$ is the identity matrix, $\mathbf{P}$ is a matrix with elements p_{nm}, $\mathbf{Q}$ is the column vector containing elements q_m, given by

$$p_{mn}=\frac{-ja_na_m\sin(\varsigma_nd)\exp(j\varsigma_md)}{2\pi a\varsigma_m}(I_1+I_2), \quad (7)$$

$$q_n=\frac{2jk_za_n\left[(-1)^n\exp(jk_xa)-\exp(-jk_xa)\right]\exp(j\varsigma_nd)}{a\left(a_n^2-k_x^2\right)\varsigma_n}, \quad (8)$$

$$I_1(m,n)=\int_0^{\infty}-\left[v(-2j+v)\right]^{1/2}\exp(-2vak_0)\cdot\frac{4j(-1)^n\exp(2jak_0)}{k_0^2\left[(1+jv)^2-\alpha^2\right]\left[(1+jv)^2-\beta^2\right]}dv, \quad (9)$$

$$I_2(m,n)=\frac{4j}{k_0^2}\left(\frac{\sqrt{1-\alpha^2}}{\alpha\left(\alpha^2-\beta^2\right)}\sin^{-1}\alpha-\frac{\sqrt{1-\beta^2}}{\beta\left(\alpha^2-\beta^2\right)}\sin^{-1}\beta\right), \quad (10)$$

$$\alpha=a_m/k_0, \quad (11)$$

$$\beta=a_n/k_0, \quad (12)$$

With the coefficients c_n, the electric field at the interface $z=0$ can be calculated via (5) and the far-field scattered electric field amplitude is evaluated based on Fresnel-Kirchhoff diffraction integral, given by

$$E_y(x',y',z_0)=\frac{1}{i\lambda}\iint_A E_y(x,y,0)\frac{\exp\left[ik_0r(x',y',x,y)\right]}{r(x',y',x,y)}dxdy, \quad (13)$$

where x' and y' are the x-coordinate and y-coordinate at the observation plane $z=z_0$, A is the area of the aperture, $r(x',y',x,y)$ is the distance. With the assumption of paraxial diffraction, $r(x',y',x,y)$ can be approximated to be

$$r(x',y',x,y)\approx z_0+\frac{(x'-x)^2+(y'-y)^2}{2z_0}. \quad (14)$$

Substituting (13) into (1), one can numerically obtain the detected scattering intensity.

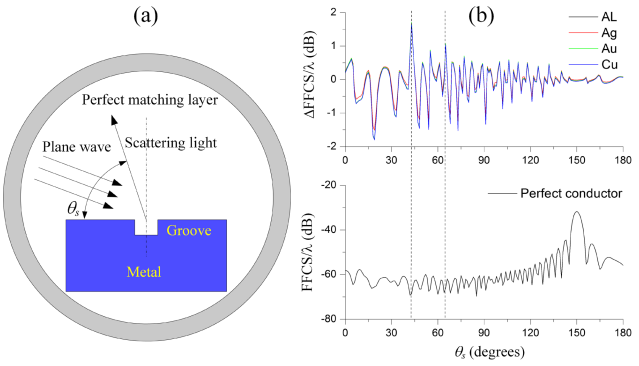

FIGURE 2. (a) FEM simulation configuration. (b) FFCS for a perfect conductor and different metals. ΔFFCS: the FFCS deviation between metals and a perfect conductor.

As rigorous solutions require perfect conductivity, it is worth evaluating the influences of finite conductivity of a real metal on the scattering light distribution. A simulation based on finite element method is performed to study the far-field scattering light distribution in commercial COMSOL Multiphysics. Figure 2(a) shows the simulation configuration of the two-dimensional scattering problem. The illumination wavelength is set to be 1 μm and the angle between the beam and the normal direction of surface is 60°. The groove parameters are $2a=0.2$ μm and $d=1$ μm. Figure 2(b) shows the far-field cross sections (FFCS) of scattering light for a perfect conductor and different metals provided by COMSOL. The electric conductivities ranges from 3.5e7 S/m for aluminum to 6.3e7 S/m for silver to infinity for a perfect conductor. The average absolute FFCS deviations are all less than 0.25 dB for the four metals. Therefore, despite of the assumption of perfect conductivity, the modal theory described here can still work for common metals with acceptable precision, including aluminum, copper, silver and gold. To further extend the work in optical components made of glass, geometrical optics approximation in [36] can be used to complement the modal theory.

III. INVERSE MODELING

As it is difficult to analytically derive the explicit expression to describe the relationship between groove parameters and intensity vectors, the inverse modeling is transformed into an optimization problem by minimizing the deviation between target and simulated intensity vectors through optimizing the groove parameters. Since the optimization will suffer from low efficiency if it searches for the global optimum solution in the entire parameter space, a two-stage inverse modeling approach is developed for improving computational efficiency. In the first stage, a lookup table including groove parameters and corresponding intensity vectors is built and the target intensity vector is compared with each item in the table to get the groove parameters that have the most similar intensity vector. Subsequently, a repulsive PSO algorithm optimizes the groove parameters with the initial value provided by the lookup table in the second stage.

A. LOOKUP TABLE

A lookup table can be generated by simulating intensity vectors corresponding to uniformly distributed groove parameters inside the parameter space utilizing (1). A metric is necessary to evaluate the similarity between target and simulated intensity vectors. In this study, it is defined to be

$$S(a, d) = -\sum_{i=1}^{N} |I_i - J_i|, \tag{15}$$

where $\mathbf{I} = [I_1, I_2, \ldots, I_N]$ and $\mathbf{J} = [J_1, J_2, \ldots, J_N]$ are respectively the target and simulated intensity vectors. Groove parameters with the highest similarity value are transferred to the second stage as initial value for optimization.

B. REPULSIVE PSO

As a typical heuristic search method, the repulsive PSO has been applied in various scenarios. It has been proved to outperform the efficiency of standard PSO method and genetic algorithms in the inverse surface radiation problem [37]. It is employed in this paper to perform the search of optimum groove parameters. After initializing the particles randomly in the neighborhood of the initial value from the first stage, the fitness values are calculated for each particle. For conveniences, the fitness value for a specified particle is defined to be the similarity value $S(a, d)$. With these fitness values, the local and global optimum particle positions are updated and the velocity direction of particle movements in the next iteration can be obtained according to

$$v_i^{k+1} = c_0 v_i^k + c_1 r_1 \left(p_i^k - x_i^k\right) + c_2 r_2 \left(p^k - x_i^k\right) + c_3 r_3 \sum_{j=1}^{M} T_{ij}, \tag{16}$$

where v_i^k denotes the velocity of the i^{th} particle in the kth generation. C_i $(I = 0, 1, 2, 3)$ is the weight for each term in the velocity. R_i $(I = 1, 2, 3)$ is a random variable between (0, 1). p_i^k and p^k are respectively the particle positions associated with the local and global best fitness values. $x_i^k = (a, d)$ is the position of the i^{th} particle in the k^{th} generation. M is the population size. The repulsive and attractive forces T_{ij} are defined as

$$T_{ij} = \begin{cases} \left(x_j - x_i\right) \dfrac{q_i q_j}{\left\|x_i - x_j\right\|^2}, & S\left(x_i\right) < S\left(x_j\right) \\ \left(x_i - x_j\right) \dfrac{q_i q_j}{\left\|x_i - x_j\right\|^2}, & S\left(x_i\right) \geq S\left(x_j\right), \end{cases} \tag{17}$$

where q_i denotes the electric charge of the i^{th} particle, given by

$$q_i = \exp^{-1}\left(\frac{S\left(x_i\right) - S\left(p^k\right)}{\sum_{j=1}^{M}\left[S\left(x_j\right) - S\left(p^k\right)\right]}\right). \tag{18}$$

On the right-hand side of (16), the first term represents the inertial influences, the second and third terms try to pull the particle towards the direction with higher fitness value, the fourth term helps to pull the particle away from the particles with low fitness value.

The velocity for the particle swarm is updated in every generation, with which the new particle position is estimated to be

$$x_i^{k+1} = x_i^k + v_i^{k+1}. \tag{19}$$

Repeating the update of velocity and particle position until a certain convergence criterion is met or iteration number exceeds the predefined value, the particle swarm optimization algorithm aims to search the particle position with the highest fitness value in the neighborhood of initial particle position.

IV. SAMPLE RESULTS AND DISCUSSIONS

In this section, sample results of both forward and inverse modeling will be provided for different groove, illumination, and inverse modeling parameters. Both forward and inverse modeling are conducted in Matlab. A personal computer with a CPU of Intel(R) Core(TM) i7-7700U @ 3.60 GHz and 8.00 GB RAM is employed in the simulation.

A. FORWARD MODELING

The validation of forward modeling code is first examined by comparing the simulated results with the published results in the literature. The related groove and illumination parameters are $a = 0.5$ μm, $d = 0.25$ μm, $\theta_i = 90°$, $\lambda = 1$ μm. Electric field at the interface between groove and air is shown in Fig. 3 (Solid line), which is symmetric to the xOz plane and agrees well with that in [21].

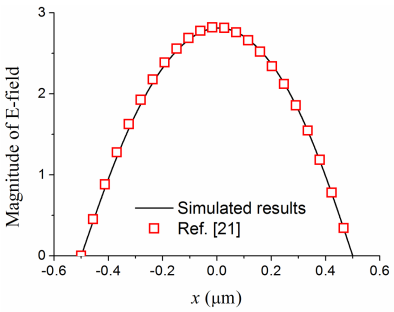

FIGURE 3. Magnitude of E-field at the interface between groove and air.

Subsequently, dependence of multi-angle light scattering on groove and illumination parameters is calculated. The scattering angle is set to be 5° and other involved parameters are $a = 2.4$ μm, $d = 0.6$ μm, $\lambda = 0.5$ μm except for explicit definition. The infinite series in (5) are truncated at the integer closest to $4a/\lambda+2$ in the following simulation. Figure 4 gives the intensity dependence of on groove widths and depths. The intensity curve associated with small width varies smoothly and stronger oscillation is observed with increase of width. From the viewpoint of geometrical optics, the scattered light is predominantly determined by the edge diffraction, indicating the width variation contributes

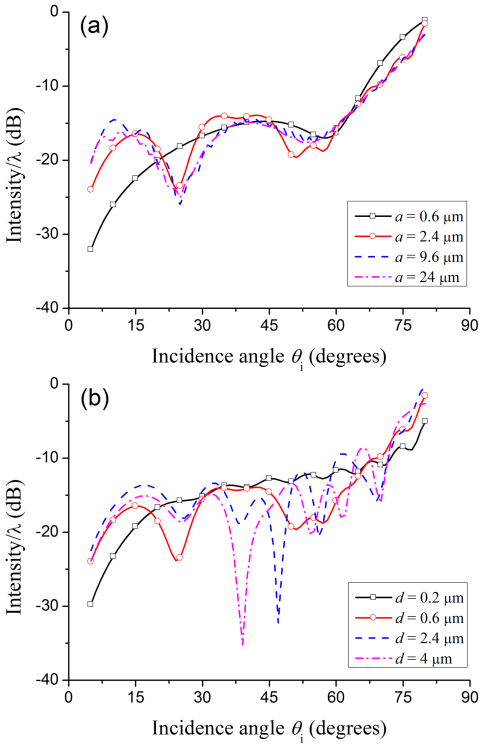

FIGURE 4. Dependence of multi-angle light scattering on groove widths and depths.

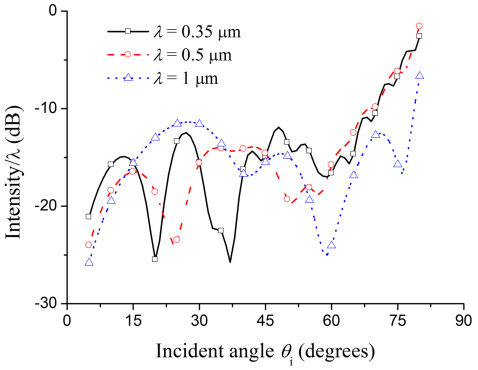

FIGURE 5. Dependence of multi-angle light scattering on wavelength.

little to scattered light. Therefore, the intensity curves change little for widths much larger than the wavelength, where geometric optics can be an approximation to the modal theory. As the element number of **P** depends on groove width, it takes longer computational time for grooves with larger widths in the modal theory, which is approximately 1.2 s for $a = 2.4\ \mu$m. The computation efficiency can be further improved by performing the calculation in the C++ language. If the width is much larger than wavelength, geometrical optics approximation can be an alternative approach to model the scattering. Likewise, the groove depths significantly affect the multi-angle scattering for oblique illumination. With the increase of the groove depth, the intensity curve becomes increasingly oscillated due to the reflection on side walls of grooves. The intensity at $\theta_i = 0°$ and 90° changes little as the side wall has little influences for the normal and grazing incidences.

Influences of illumination wavelength are presented in Fig. 5. Larger oscillation is observed for short wavelength as more modes are included in P_{mn} and Q_m, which suggests us to use short wavelengths for the measurement of grooves with small widths, since the intensity oscillation is beneficial for inverse modeling.

B. INVERSE MODELING

In this section, modeled data is employed to examine the validation of the proposed inverse modeling approach. The ranges of a and d are respectively set to be [0.1 μm, 4 μm] and [0.1 μm, 4 μm] in the simulation. Plane waves with three wavelengths of 0.35 μm, 0.5 μm, and 0.65 μm are used to provide the illumination. Three incidence angles are employed for each wavelength, where $[\lambda, \theta_i] = [0.35\ \mu$m, 10°], [0.35 μm, 25°], [0.35 μm, 40°], [0.5 μm, 15°], [0.5 μm, 30°], [0.5 μm, 45°], [0.65 μm, 20°], [0.65 μm, 35°], and [0.65 μm, 50°]. 160000 intensity vectors associated with uniform distribution of 400 widths and 400 depths are calculated to generate the lookup table. Each intensity vector contains nine elements corresponding to the nine plane waves.

TABLE 1. Searched results for a given target intensity vector.

	a (μm)	d (μm)	$\lvert S(a,d)\rvert/\lambda$ (dB)
Target	1.7431	1.3922	N/A
Result 1	1.7422	1.3889	-21.79
Result 2	1.7422	1.3985	-20.18
Result 3	1.7422	1.3794	-18.19
Result 4	1.7422	1.4080	-17.60
Result 5	1.7327	1.3889	-16.80

The performance of lookup table is first examined. As measurement noise can never be completely eliminated in a practical experiment, it has to be considered in the inverse modeling. It is shown that the intensity is generally much less for grazing incidence than the case for normal incidence in Figs. 4 and 5. The intensity of illumination light with different incidence angles should be separately adjusted to get similar intensity of scattered light and extend the dynamic range of detector. In this case, multiplicative noises are added by multiplying the intensity I_i with $\gamma = 1 + \gamma_0 \upsilon$, where υ is a random quantity uniformly distributed over the interval $[-1, 1]$ and γ_0 is a coefficient defining the standard deviation of the noise. Table 1 gives the searched results for the intensity vector corresponding to $(a, d) = (1.7431\ \mu$m, 1.3922 μm) after noise pollution ($\gamma_0 = 0.05$). As expected, the groove parameters with intensity vectors most similar to the target intensity vector are in the neighborhood of the target groove parameters.

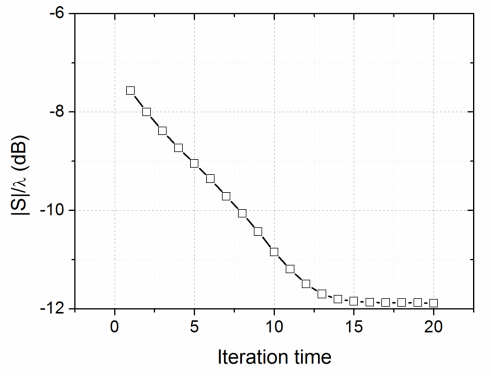

FIGURE 6. Evolution of summed fitness value of particles in the same generation over iterations in the PSO.

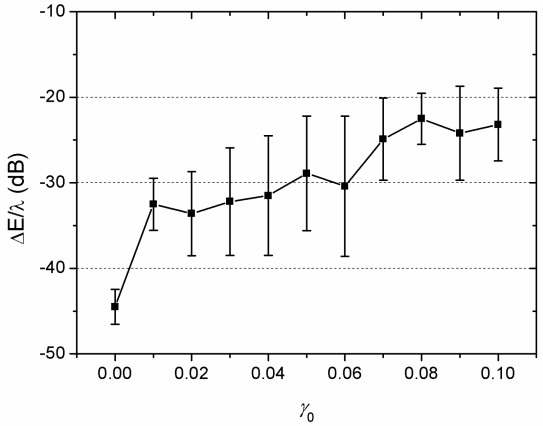

FIGURE 7. Prediction error for noise-polluted scattered light signals.

The groove parameters with the highest similarity value is then transferred to the repulsive PSO algorithm. The population size and generation are respectively set to be 50 and 20. The first-generation particle positions are generated randomly in the neighborhood of initial particle positions with $\Delta a = 0.1\ \mu$m and $\Delta d = 0.1\ \mu$m. To demonstrate the performance of PSO, the fitness value of particle swarm in the same generation is summed and its evolution over iterations is illustrated in Fig. 6. The summed fitness value increases over iterations, indicating that the particles generally move towards the position with the highest fitness value.

Theoretically, the repulsive PSO algorithm can always obtain the target groove parameters at high computational costs as long as the population size and iteration number are large enough. However, the performance of the repulsive PSO algorithm still needs to be examined for limited computational time and noise-polluted intensity vectors. The prediction error of groove parameters is adopted to quantitatively evaluate the performance, defined to be

$$\Delta E = [(a_r - a_0)^2 + (d_r - d_0)^2]^{1/2}, \tag{20}$$

where (a_r, d_r) and (a_0, d_0) are respectively the retrieved and target groove parameters. The intensity vector associated with the target groove parameters in Table 1 is randomly polluted by noises and the repulsive PSO is subsequently conducted to retrieve groove parameters with the first-generation particle positions randomly generated in the neighborhood of target groove parameters in Table 1. The procedure is repeated 11 times for each γ_0 and an error bar is generated to show the influences of randomness on prediction error. It takes approximately 15 minutes for one-time optimization. Further acceleration based on parallel computing is expected for real-time measurements. Results are shown in Fig. 7. Although the prediction error generally increases with increase of γ_0, the average prediction error is less than $\lambda/100$ at $\gamma_0 = 0.1$, demonstrating that the multi-angle light scattering technique is a reliable approach to quantitatively characterize the rectangular groove even under severe noise influences. However, high signal-to-noise ratio is still desirable in the measurement in case the lookup table gives false initial groove parameters.

V. CONCLUSION

In conclusion, a numerical procedure is developed towards characterization of rectangular grooves on a metallic surface based on multi-angle light scattering. The program includes both forward and inverse modeling of light scattering by rectangular grooves. In the forward modeling, the modal theory is adopted to solve the electromagnetic scattering problem. A two-stage approach using lookup table and repulsive PSO algorithm is developed to retrieve the groove parameters from multi-angle light scattering measurements. Both noise-free and noise-polluted scenarios are simulated to demonstrate the method. In both cases, the lookup table and repulsive PSO algorithm can respectively provide rough and precise estimations of groove parameters. As the proposed approach is designed in accordance with practical experiments, it can give indications to experimental systems for quantitative characterization of rectangular grooves on a metallic surface.

REFERENCES

[1] Y. Arieli, S. Epshtein, I. Yakubov, Y. Weitzman, G. Locketz, and A. Harris, "Surface measurements by white light spatial-phase-shift imaging interferometry," *Opt. Express*, vol. 22, no. 13, pp. 15632–15638, Jun. 2014.

[2] T. Widjanarko, J. M. Huntley, and P. D. Ruiz, "Single-shot profilometry of rough surfaces using hyperspectral interferometry," *Opt. Lett.*, vol. 37, no. 3, pp. 350–352, Feb. 2012.

[3] S. Freund, A. Hinaut, R. Pawlak, S.-X. Liu, S. Decurtins, E. Meyer, and T. Glatzel, "Morphology change of C60 islands on organic crystals observed by atomic force microscopy," *ACS Nano*, vol. 10, no. 6, pp. 5782–5788, Jun. 2016.

[4] S. Helmig and K. V. Gothelf, "AFM imaging of hybridization chain reaction mediated signal transmission between two DNA origami structures," *Angew. Chem.*, vol. 129, no. 44, pp. 13821–13824, Oct. 2017.

[5] *Performance Specification: Optical Components for Fire Control Instruments; General Specification Governing The Manufacture, Assemble, and Inspection*, document MIL-PRF-13830B, 1997.

[6] *Optics and Photonics—Preparation of Drawings for Optical Elements and Systems—Part 7: Surface Imperfection Tolerances*, Standard ISO 10110-7:2008, 2009.

[7] D. M. Aikens, "Objective measurement of scratch and dig," in *Proc. Imag. Appl. Opt. Tech. Papers, OSA Tech. Dig., Opt. Soc. Amer.*, 2012, Paper OTu2D.5, doi: 10.1364/OFT.2012.OTu2D.5.

[8] D. Kiefhaber, F. Etzold, J. M. Asfour, and A. Warken, "Automated surface quality inspection with ARGOS: A case study," *Proc. SPIE*, vol. 10326, Jun. 2017, Art. no. 103260T.

[9] D. Liu, S. Wang, P. Cao, L. Li, Z. Cheng, X. Gao, and Y. Yang, "Dark-field microscopic image stitching method for surface defects evaluation of large fine optics," *Opt. Express*, vol. 21, no. 5, pp. 5974–5987, Mar. 2013.
[10] J. Dong, "Line-scanning laser scattering system for fast defect inspection of a large aperture surface," *Appl. Opt.*, vol. 56, no. 25, pp. 7089–7098, Sep. 2017.
[11] R. Chen, N. Ilasi, and S. S. Sekulic, "Absolute molecular weight determination of hypromellose acetate succinate by size exclusion chromatography: Use of a multi angle laser light scattering detector and a mixed solvent," *J. Pharmaceutical Biomed. Anal.*, vol. 56, no. 4, pp. 743–748, Dec. 2011.
[12] B. J. Bauer, J. A. Fagan, E. K. Hobbie, J. Chun, and V. Bajpai, "Chromatographic fractionation of SWNT/DNA dispersions with on-line multi-angle light scattering," *J. Phys. Chem. C*, vol. 112, no. 6, pp. 1842–1850, Feb. 2008.
[13] O. Link, D. R. Snelling, K. A. Thomson, and G. J. Smallwood, "Development of absolute intensity multi-angle light scattering for the determination of polydisperse soot aggregate properties," *Proc. Combustion Inst.*, vol. 33, no. 1, pp. 847–854, 2011.
[14] Z. Hu, C. Ye, W. Mi, Y. Zhao, C. Quan, W. W. Li, H. Li, and H. Hang, "Light-scattering detection within the difficult size range of protein particle measurement using flow cytometry," *Nanoscale*, vol. 10, no. 41, pp. 19277–19285, Oct. 2018.
[15] P. Goktas, I. O. Sukharevsky, F. A. Kuypers, O. Yalcin, A. Altintas, and S. Larkin, "Image-based flow cytometry and angle-resolved light scattering to define the sickling process," *Cytom. A*, vol. 95, no. 5, pp. 488–498, 2019.
[16] W. Zhang, Y. Tian, X. Hu, S. He, Q. Niu, C. Chen, S. Zhu, and X. Yan, "Light-scattering sizing of single submicron particles by high-sensitivity flow cytometry," *Anal. Chem.*, vol. 90, no. 21, pp. 12768–12775, Nov. 2018.
[17] M. Ogawa, M. Nakada, R. Katayama, M. Okada, and M. Itoh, "Analysis of scattering light from magnetic material with Land/Groove by three-dimensional boundary element method," *Jpn. J. Appl. Phys.*, vol. 35, no. 1, pp. 336–341, Jan. 1996.
[18] W.-H. Yeh, L. Li, and M. Mansuripur, "Computation of effective groove depth in an optical disk with vector diffraction theory," *Appl. Opt.*, vol. 39, no. 2, pp. 316–323, Jan. 2000.
[19] S. Zhang, H. Liu, and G. Mu, "Electromagnetic enhancement by a periodic array of nanogrooves in a metallic substrate," *J. Opt. Soc. Amer. A, Opt. Image Sci.*, vol. 28, no. 5, pp. 879–886, May 2011.
[20] C.-Y. Ho, B.-C. Chen, and Y.-H. Tsai, "Scattering signals of monochromatic light incident on a rectangular microchannel," *Comput. Math. Appl.*, vol. 64, no. 5, pp. 1514–1521, Sep. 2012.
[21] M. A. Basha, S. K. Chaudhuri, S. Safavi-Naeini, and H. J. Eom, "Rigorous formulation for electromagnetic plane-wave scattering from a general-shaped groove in a perfectly conducting plane," *J. Opt. Soc. Amer. A, Opt. Image Sci.*, vol. 24, no. 6, pp. 1647–1655, Jun. 2007.
[22] T. J. Park, K. Yoshitomi, and H. J. Eom, "Analysis of TM scattering from finite rectangular grooves in a conducting plane," *J. Opt. Soc. Amer. A, Opt. Image Sci.*, vol. 10, no. 5, pp. 905–911, May 1993.
[23] C. J. R. Sheppard, "Imaging of random surfaces and inverse scattering in the Kirchhoff approximation," *Wave. Random Media*, vol. 8, no. 1, pp. 53–66, 1998.
[24] M. J. Boedigheimer and J. Ferbas, "Mixture modeling approach to flow cytometry data," *Cytometry Part A*, vol. 73A, no. 5, pp. 421–429, May 2008.
[25] D. Macías, G. Olague, and E. R. Méndez, "Inverse scattering with far-field intensity data: Random surfaces that belong to a well-defined statistical class," *Waves Random Complex Media*, vol. 16, no. 4, pp. 545–560, Nov. 2006.
[26] R. J. W. Hodgson, "Genetic algorithm approach to particle identification by light scattering," *J. Colloid Interface Sci.*, vol. 229, no. 2, pp. 399–406, Sep. 2000.
[27] N. Riefler and T. Wriedt, "Intercomparison of inversion algorithms for particle-sizing using MIE scattering," *Part. Part. Syst. Characterization*, vol. 25, no. 3, pp. 216–230, 2008.
[28] B. Barkey, S. E. Paulson, and A. Chung, "Genetic algorithm inversion of dual polarization polar nephelometer data to determine aerosol refractive index," *Aerosol Sci. Technol.*, vol. 41, no. 8, pp. 751–760, Jul. 2007.
[29] Z. Wang, Z. Ulanowski, and P. H. Kaye, "On solving the inverse scattering problem with RBF neural networks: Noise-free case," *Neural Comput. Appl.*, vol. 8, no. 2, pp. 177–186, May 1999.
[30] E. O. Salawu, E. Hesse, C. Stopford, N. Davey, and Y. Sun, "Applying machine learning methods for characterization of hexagonal prisms from their 2D scattering patterns—An investigation using modelled scattering data," *J. Quant. Spectrosc. Radiat. Transf.*, vol. 201, pp. 115–127, Nov. 2017.
[31] Z. Cao, F. Cui, F. Xian, C. Zhai, and S. Pei, "A hybrid approach using machine learning and genetic algorithm to inverse modeling for single sphere scattering in a Gaussian light sheet," *J. Quant. Spectrosc. Radiat. Transf.*, vol. 235, pp. 180–186, Sep. 2019.
[32] N. Jin and Y. Rahmat-Samii, "Advances in particle swarm optimization for antenna designs: Real-number, binary, single-objective and multiobjective implementations," *IEEE Trans. Antennas Propag.*, vol. 55, no. 3, pp. 556–567, Mar. 2007.
[33] M.-T. Pham, D. Zhang, and C. S. Koh, "Multi-guider and cross-searching approach in multi-objective particle swarm optimization for electromagnetic problems," *IEEE Trans. Magn.*, vol. 48, no. 2, pp. 539–542, Feb. 2012.
[34] A. Semnani, M. Kamyab, and I. T. Rekanos, "Reconstruction of one-dimensional dielectric scatterers using differential evolution and particle swarm optimization," *IEEE Geosci. Remote Sens. Lett.*, vol. 6, no. 4, pp. 671–675, Oct. 2009.
[35] T. Wei, F. Yu, G. Huang, and C. Xu, "A Particle-Swarm-Optimization-Based parameter extraction routine for three-diode lumped parameter model of organic solar cells," *IEEE Electron Device Lett.*, vol. 40, no. 9, pp. 1511–1514, Sep. 2019.
[36] Z. Cao, F. Cui, F. Xian, J. Li, and S. Pei, "Geometrical optics approximation for plane-wave scattering by a rectangular groove on a surface," *Appl. Opt.*, vol. 59, no. 8, pp. 2600–2605, Mar. 2020.
[37] K. H. Lee, "Application of repulsive particle swarm optimization for inverse heat conduction problem–Parameter estimations of unknown plane heat source," *Int. J. Heat Mass Transf.*, vol. 137, pp. 268–279, Jul. 2019.

ZHAOLOU CAO was born in Jiangsu, China, in 1988. He received the B.S. degree in mechanical engineering and the Ph.D. degree in measurement technology and instruments from the University of Science and Technology of China, in 2009 and 2014, respectively. He is currently an Associate Professor with the Nanjing University of Information Science and Technology. He has authored or coauthored over 30 publications (articles and inventions). His research interests include electromagnetic theory, optical metrology, and imaging techniques.

FENPING CUI was born in Anhui, China, in 1981. She received the B.S. degree in biology education from Anhui Normal University, in 2002, and the M.S. degree from the Anhui Institute of Optics and Fine Mechanics, in 2005. She has been a Senior Engineer with the Nanjing University of Information Science and Technology, since 2006. She has authored or coauthored over 30 publications (articles and inventions). Her research interests include environment optics and optical measurement.

FENGLIN XIAN was born in Jiangsu, China, in 1986. He received the B.S. degree in physics from Xinjiang University, in 2009, and the Ph.D. degree in optical engineering from the Nanjing University of Science and Technology, in 2015. He is currently an Assistant Professor with the Nanjing University of Information Science and Technology. He has authored or coauthored over 20 publications (articles and inventions). His research interests include electromagnetic theory, optical material, and nano-optics.

SHIXIN PEI was born in Gansu, China, in 2000. He received the B.S. degree in chemistry education from Northwest Normal University, in 2000, and the Ph.D. degree from the Anhui Institute of Optics and Fine Mechanics, in 2005. He is currently a Professor with the Nanjing University of Information Science and Technology. He has authored or coauthored over 50 publications (articles and inventions). His research interests include environment optics, electromagnetic theory, and physics education.

JINHUA LI was born in Henan, China, in 1984. She received the B.S. degree in physics from Xinyang Normal University, in 2005, the M.S. degree in theoretical physics from Ningbo University, in 2008, and the Ph.D. degree in optics from The University of Hong Kong, in 2013. She is currently an Associate Professor with the Nanjing University of Information Science and Technology. She has authored or coauthored over 30 publications. Her research interests include electromagnetic theory and nonlinear optics.

HUICHUN YE was born in Guangxi, China, in 1986. He received the B.S. degree in mechanical engineering and the Ph.D. degree in measurement technology and instruments from the University of Science and Technology of China, in 2009 and 2014, respectively. He is currently a Lecturer with the University of Science and Technology of China. He has authored or coauthored over 20 publications (articles and inventions). His research interests include nanofabrication and finite element analysis.